Oxidative Potential Associated with Urban Aerosol Deposited into the Respiratory System and Relevant Elemental and Ionic Fraction Contributions

Maurizio Manigrasso [1], Giulia Simonetti [2], Maria Luisa Astolfi [2], Cinzia Perrino [3], Silvia Canepari [2], Carmela Protano [4], Arianna Antonucci [4], Pasquale Avino [5] and Matteo Vitali [4,*]

[1] Department of Technological Innovations, INAIL, Via Roberto Ferruzzi 38, 00143 Rome, Italy; m.manigrasso@inail.it

[2] Chemistry Department, Sapienza University of Rome, P.le Aldo Moro 5, 00185 Rome, Italy; giulia.simonetti@uniroma1.it (G.S.); marialuisa.astolfi@uniroma1.it (M.L.A.); silvia.canepari@uniroma1.it (S.C.)

[3] C.N.R. Institute of Atmospheric Pollution Research, Via Salaria, km 29, 300, Monterotondo St., 00015 Rome, Italy; perrino@iia.cnr.it

[4] Department of Public Health and Infectious Diseases, Sapienza University of Rome, P.le Aldo Moro 5, 00185 Rome, Italy; carmela.protano@uniroma1.it (C.P.); arianna.antonucci@uniroma1.it (A.A.)

[5] Department of Agricultural, Environmental and Food Sciences (DiAAA), University of Molise, 86100 Campobasso, Italy; avino@unimol.it

[*] Correspondence: matteo.vitali@uniroma1.it

Abstract: Size-segregated aerosol measurements were carried out at an urban and at an industrial site. Soluble and insoluble fractions of elements and inorganic ions were determined. Oxidative potential (OP) was assessed on the soluble fraction of Particulate Matter (PM) by ascorbic acid (AA), dichlorofluorescein (DCFH) and dithiothreitol (DTT) assays. Size resolved elemental, ion and OP doses in the head (H), tracheobronchial (TB) and alveolar (Al) regions were estimated using the Multiple-Path Particle Dosimetry (MPPD) model. The total aerosol respiratory doses due to brake and soil resuspension emissions were higher at the urban than at the industrial site. On the contrary, the doses of anthropic combustion tracers were generally higher at the industrial site. In general, the insoluble fraction was more abundantly distributed in the coarse than in the fine mode and vice versa for the soluble fraction. Consequently, for the latter, the percent of the total respiratory dose deposited in TB and Al regions increased. Oxidative potential assay (OP^{AA}) doses were distributed in the coarse region; therefore, their major contribution was in the H region. The contribution in the TB and Al regions increased for OP^{DTT} and OP^{DCFH}.

Keywords: size resolved oxidative potential; traffic; soil dust; anthropic combustion; secondary aerosol; biomass burning; respiratory doses; MPPD

1. Introduction

Particulate matter (PM) is a well-known risk factor for human health, involved in the pathogenesis of cardiovascular [1], respiratory [2] and neurodegerative diseases [3]. Exposure to PM during pregnancy has been also associated with adverse outcomes for intrauterine development such as low birth weight, preterm birth and small for gestational age births [4]. In addition, the International Agency for the Research on Cancer, in 2013, classified PM in outdoor air pollution as a carcinogenic to humans (Group 1) [5]. Despite the great number of the negative effects on human health associated with PM exposure, etiopathogenetic mechanisms are still unclear and under evaluation. As is well-known, one of the most accredited hypothesis considers the oxidative stress as the primum movens of the

PM-related diseases development; in particular, Reactive Oxygen Species (ROS) seem to play a central role in the etiopathogenesis of the diseases, due to their unbalanced excess that causes oxidative stress, resulting in injury to cells and tissues in the respiratory tract [6]. Acellular Oxidative Potential (OP) assays are frequently used to estimate the PM ability to oxidize target molecules, integrating the contributions due to different chemical species [7,8].

PM size distribution is strictly related to both emission sources and related adverse effects. The study of PM dimensional distribution and of its chemical composition gives information about the sources. It is well-known that coarse PM originates mainly from resuspension processes or mechanical shearing, while fine PM derives from combustive processes or from secondary formation in the atmosphere [9]. Regarding the adverse health effect of PM, its size distribution influences the ability of particles to penetrate in the respiratory system [10]. At the site of particles deposition into the respiratory tract, different health endpoints can be induced depending on their chemical composition.

Within this context, the aim of this study is to estimate the penetration of the PM size fractions, collected by a multistage impactor, into the head (H), tracheobronchial (TB) and alveolar (Al) regions of the respiratory system and to assess to what extent such penetration may change, depending on the different PM emissive sources. The PM's capability to induce oxidative processes was estimated in each region of the respiratory tract by ascorbic acid, dithiothrietol and dichlorofluorescein oxidative potential assays (OP^{AA}, OP^{DTT} and OP^{DCFH}, respectively).

2. Experiments

2.1. Aerosol Sampling

An urban and an industrial area were selected to carry out aerosol samplings. The first one (from 16 to 30 March 2017), characterized by intense traffic emissions, was in downtown Rome (Google Earth co-ordinates: Lat. 41.902433° Long. 12.517505°). The second one (from 17 February to 9 March 2017), characterized by both industrial and traffic emissions, was in the Po valley, near Ferrara and close to an industrial area (Google Earth co-ordinates: Lat. 44.848774° Long. 11.561354°). Size-segregated aerosol samples were collected on 47 mm, 2.0 μm pore size Teflon filters by means of Uniform Deposition Impactors (MOUDI; mod. 110.R, MSP) operating at the flow rate of 30 L min^{-1}, with aerodynamic diameter cut-sizes of 0.18, 0.32, 0.56, 1.0, 1.8, 3.2, 5.6, 10 and 18 μm. Two impactors were used in parallel at each site. Further details on the sampling campaigns are reported in [11].

2.2. Chemical Analysis

The detailed extraction and chemical analysis procedure is described in [11] and in [12]. In brief, the mass aerosol concentration was determined by weighing with a microbalance (1 μg sensitivity, mod. ME5, Sartorius). The Teflon filters were extracted in deionized water and filtered on 0.45 μm pore size nitrocellulose membranes. In different aliquots of the soluble fraction inorganic ions were determined by ion chromatography and soluble elements by inductively coupled plasma-mass spectrometry (ICP-MS). The insoluble fraction of the samples was digested by a microwave oven in a HNO_3/H_2O_2 mixture (2:1), and analyzed by ICP-MS to determine the same elements as for the soluble fraction. Instrumental operative conditions are detailed in [13].

The oxidative potential (OP) was determined on the soluble fraction by the dichlorofluorescein diacetate (DCFH), dithiothreitol (DTT) and ascorbic acid (AA) assays. These three methods are among the most frequently adopted in the literature; each of them is sensitive toward different PM components. In particular, AA was demonstrated to respond mainly to elements, such as copper and iron, present in the non-combustive vehicular emission, whereas DTT is also sensitive toward secondary organic species. Both these assays measure the rate of depletion of reducing species that are naturally present in vivo (AA) or are proxy of naturally occurring antioxidants (DTT). On the other hand, DCHF assay measures particle-bound reactive oxygen species [7]. As they represent different mechanisms, their combined use is often suggested [14].

DTT and AA absorbance was recorded by UV-Vis spectroscopy at 412 nm and 216 nm, respectively. The relevant oxidative potential (OP^{DTT} and OP^{AA}) were expressed as the AA or DTT consumption rate per sampled volume (nmol min^{-1} m^{-3}). OP^{DCFH} was measured by a fluorescence detector (excitation wavelength: 427 nm), through the emitted radiation at 530 nm. The calibration curve was carried out with standard H_2O_2 solutions. OP^{DCFH}, expressed as nmol H_2O_2 per sampled volume, were obtained by converting the fluorescence intensity into H_2O_2 equivalents. Analytical procedures are described in more detail in supplementary material S1.

Chemical analysis results and OP data are reported and discussed in terms of source attribution in [11]. For all the measured parameters, the differences between values obtained from the two impactors placed in parallel were lower than 15%. Relying on such a database, dosimetry evaluations were carried out in the present study.

2.3. Aerosol Dosimetry

Aerosol doses deposited after 1h exposure time in the H, TB and Al regions of the respiratory system were determined as function of the mid- size class aerodynamic diameter (d_{ai}) of the MOUDI impactor (Equation (1)), for each analyte (*an.*), whether it be an analyzed element or OP, or particle mass concentration (*m*). For the size class below 0.18 μm the 24 h average value of the geometric mean diameter estimated in downtown Rome was adopted (0.055 μm) [15]. For the elements analyzed and for particle mass concentration the doses were expressed in ng and in μg, respectively. For OP^{DTT} and OP^{AA} they were expressed in nmol min^{-1} and for OP^{DCFH} in nmol H_2O_2. The particle regional deposition fractions per ($F^R(d_{ai})$) as a function of d_{ai} were estimated using the Multiple-Path Particle Dosimetry model (MPPD v3.01, ARA 2015, ARA, Arlington, VA, USA) [16]. The 60th percentile human stochastic lung was considered along with the following settings: (i) a uniformly expanding flow, (ii) an upright body orientation, and (iii) nasal breathing with a 0.5 inspiratory fraction and no pause fraction. Moreover, the following parameters were used for a Caucasian adult male under light work physical activity, based on the ICRP report [17]: (i) a functional residual capacity (FRC) of 3300 mL, (ii) an upper respiratory tract (URT) volume equal to 50 mL, (iii) a breathing frequency (B) of 20 min^{-1}, and (iv) an air volume inhaled during a single breath (tidal volume, V_t) of 1.25 L.

$$D^R(an., d_{ai}) = F^R(d_{ai}) \times C(an., d_{ai}) \times V_t \times 60B \quad (R = H, TB, Al), \tag{1}$$

The total doses deposited into the respiratory system as s function of d_{ai} were estimated by Equation (2):

$$D^{Tot}(an., d_{ai}) = D^H(an., d_{ai}) + D^{TB}(an., d_{ai}) + D^{Al}(an., d_{ai}), \tag{2}$$

The total regional doses as functions of d_{ai} were calculated by Equation (3), where the summation is carried out over the MOUDI size classes:

$$D_{Tot}^R(an.) = \sum_i D^R(an, d_{ai}) \quad (R = H, TB, Al), \tag{3}$$

The total doses deposited into the respiratory system were calculated according Equation (4):

$$D_{Tot}^{Tot}(an.) = \sum_i D^{Tot}(an, d_{ai}), \tag{4}$$

3. Results and Discussion

Regional doses were calculated in terms of total aerosol mass and of specific components of atmospheric aerosol. The contributions of the different emission sources were addressed referring to tracer components for each of them: 1) Insoluble fraction of Cu and Sb, due to brake pads contribution, were used to trace non-combustive traffic emissions. 2) Insoluble fraction of Ti and Ce for soil dust resuspension. 3) Soluble fraction of As, Cr and Ni for anthropic emission sources, including industrial

emissions. 4) NO_3^-, SO_4^{2-} and NH_4^+, for secondary inorganic aerosol, 5) K^+ and Rb (soluble fraction) for biomass burning [18].

3.1. Total Aerosol Mass Respiratory Doses

Figure 1 describes the particle mass regional ($D^R(m, d_{ai})$) and total ($D_{Tot}^{Tot}(m)$) doses estimated for the sites in downtown Rome and Ferrara. Great part of $D_{Tot}^{Tot}(m)$ was deposited in the H region, 84% and 81% respectively at the two sites. This occurs because of the efficient filtrating action of the H region toward fine and coarse particles. At both sites almost the same doses ($D_{Tot}^{Tot}(m)$), about 20 µg, were estimated after 1h exposure. However, there were some differences in the relevant size distributions ($D^{Tot}(m, d_{ai})$) that are due to the different emission sources and to the orographic and meteo-climatic characteristics of the two sites. Close to the Ferrara site, in addition to vehicular traffic and domestic heating, industrial emissions as well are present. Moreover, pollutants tend to stagnate in the Po basin, where this site is located, because of both the Alps and the Apennine mountains surrounding it and the frequent atmospheric stability conditions that hinder their dispersion [18,19]. As a consequence, aerosol undergoes coagulation, condensation growth and secondary formation to greater extent than in Rome. Therefore, the $D^{Tot}(m, d_{ai})$ size distribution is broad, extending from sub-micron to coarse particles with a maximum in the fine mode at an aerodynamic diameter (1.0–1.8 µm) greater than in Rome (0.56–1.0 µm) and is 3-fold more abundant. On the contrary, in Rome $D^{Tot}(m, d_{ai})$ is mainly distributed in the coarse mode, because of road dust- resuspension of greater entity than at the Ferrara site, due to the more intense traffic.

These differences have consequences on the site of particle deposition within the respiratory system. Indeed, the aerosol dose deposited in the H region is greater for the Rome than for Ferrara dataset, whereas the opposite occurs for the TB and the Al doses. It is worth observing that although such differences are slight in term of mass (about 0.2 and 0.4 µg, respectively), they are expected to be more important if expressed on number metric, because smaller particles contribute to greater extent to aerosol number concentration but to minor extent to aerosol mass. Moreover, considering that aerosol chemical components are distributed in different size classes depending on their emission sources and physical-chemical transformation in atmosphere, for them as well differences are expected in their site of deposition into the respiratory system.
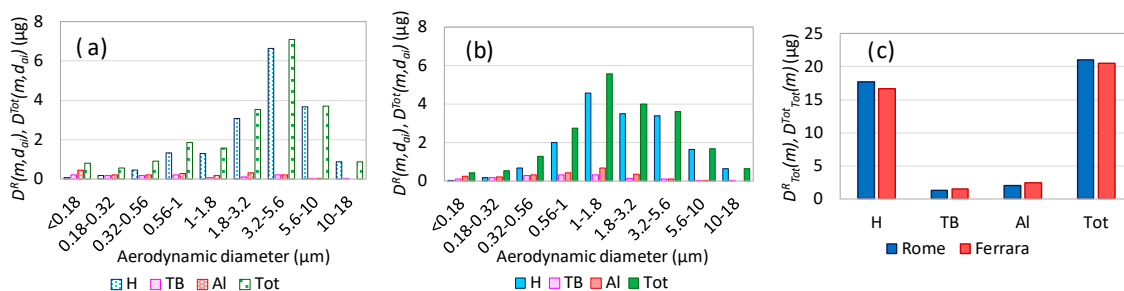

Figure 1. $D^R(m, d_{ai})$ and $D^{Tot}(m, d_{ai})$ doses at the Rome (**a**) and Ferrara (**b**) sites, relevant $D_{Tot}^R(m)$ and ($D_{Tot}^{Tot}(m)$ doses (**c**).

3.2. Aerosol Respiratory Doses from Brake Pads Abrasion

Figure 2 shows the $D^R(an., d_{ai})$ and $D^{Tot}(an., d_{ai})$ size distributions together with the $D_{Tot}^R(an.)$ and $D_{Tot}^{Tot}(an.)$ doses, for the Cu insoluble fraction after 1 h exposure at the Rome and Ferrara sites. A similar behavior was also observed in the insoluble fraction of Sb (Figure S1 in the Supplementary Material), Fe, and Sn. All these elements are reliable tracers of brake pads wear contribution and are mainly present in the coarse fractions with maximum ($D^{Tot}(an., d_{ai})$) in the 1.8–5.6 µm size range.
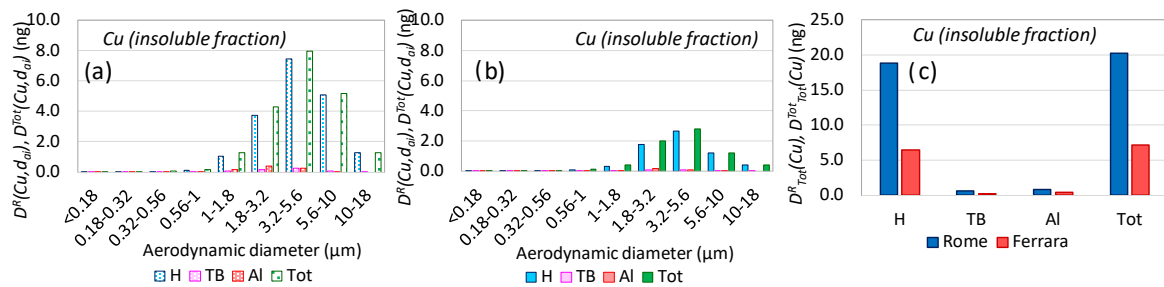
Figure 2. $D^R(Cu, d_{ai})$ and $D^{Tot}(Cu, d_{ai})$ doses at the Rome (**a**) and Ferrara (**b**) sites, relevant $D_{Tot}^R(Cu)$ and $D_{Tot}^{Tot}(Cu)$ doses (**c**) for Cu insoluble fraction.

Due to the more intense vehicular traffic, $D_{Tot}^{Tot}(an.)$ doses were higher at the Rome than at the Ferrara site: 20.3 ng and 1.0 ng at the Rome site, 7.2 ng and 0.4 ng at the Ferrara site, for Cu and Sb respectively.

The same doses as Figure 2 and Figure S1, referred to the Cu and Sb soluble fractions are reported in Figures S2 and S3 of the supplementary material. Their size distributions are shifted toward the fine region, due to the higher contribution of combustive sources to the soluble fraction of both the elements [11]. In particular, about 29%, 37% of the insoluble fraction and 56%, 87% of the soluble fraction was below 2.5 μm aerodynamic diameter respectively for Cu and Sb, at the Rome site. Such percentages were 38%, 81% for the insoluble fraction and 56%, 90% for the soluble fraction at the Ferrara site, where the fine contribute from industrial emission was higher. Such differences directly affected the partition of the two metals in the regions of the respiratory system. For the insoluble fraction, 3.0%, 4.3% at Rome and 3.6%, 5.6% of Cu at Ferrara and 5.1%, 7.6% at Rome and 8.4%, 14.4% of Sb were deposited in the H and the Al regions, respectively. For the soluble fraction, such percentages rose to 4.8%, 8.0% at Rome and 4.6%, 7.8% at Ferrara for Cu and 12.6%, 18.4% at Rome and 11.6%, 18.2% for Sb, respectively.

$D_{Tot}^{Tot}(Cu)$ and $D_{Tot}^{Tot}(Sb)$ doses for the soluble fraction were lower than the relevant doses for the insoluble fractions: 3.3 ng and 0.25 ng at the Rome site, 3.1 ng and 0.29 ng at the Ferrara site, respectively. Differently from the insoluble fractions, $D_{Tot}^{Tot}(an.)$ for the soluble fractions at the two sites were almost similar for Cu and higher at the Ferrara than at Rome site for Sb, because its soluble fraction is markedly affected by industrial emissions.

3.3. Aerosol Respiratory Doses from Soil Dust Resuspension

Figure 3 shows the $D^R(an., d_{ai})$ and $D^{Tot}(an., d_{ai})$ size distributions together with the $D_{Tot}^R(an.)$ and $D_{Tot}^{Tot}(an.)$ doses, for the Ti insoluble fractions after 1 h exposure at the Rome and Ferrara sites. Similar behavior was observed for the other tracers of soil dust resuspension (Al and Ce, Figures S4 and S5 of supplementary material, respectively).
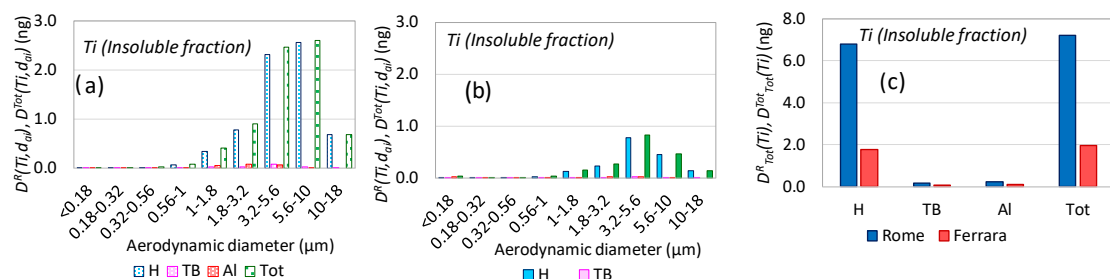

Figure 3. $M^R(Ti, d_{ai})$ and $M^{Tot}(Ti, d_{ai})$ doses at the Rome (**a**) and Ferrara (**b**) sites, relevant $M_{Tot}^R(Ti)$ and $M_{Tot}^{Tot}(Ti)$ doses (**c**) for Ti insoluble fraction.

Aerosol doses due to the resuspension of crustal material were by far higher at the Rome than at the Ferrara site. $D_{Tot}^{Tot}(an.)$ for the insoluble fraction of Al, Ti and Ce were respectively 190, 7.2 and 0.70 ng at the Rome site and 43, 2.0 and 0.1 ng at the Ferrara site, coherently with the more intense

vehicular traffic and the lower relative humidity that facilitate dust resuspension at the Rome site. At both sites $D^R(an., d_{ai})$ and $D^{Tot}(an., d_{ai})$ size distribution displayed a mode in the coarse region at 3.2–5.6 μm (Al) and 5.6–10 μm (Ti and Ce) at the Rome site and at 3.2–5.6 μm (Al, Ti, Ce) at the Ferrara site. Therefore, as for dust brake emissions, $D^{TB}_{Tot}(an.)$ and $D^{Al}_{Tot}(an.)$ doses represented a small percentage of $D^{Tot}_{Tot}(an.)$, on average 2.8% (TB region), 3.6% (Al region) at the Rome site, 3.6% (TB) and 5.2% (Al) at the Ferrara site.

As already observed for Cu and Sb, the soluble fractions of Al, Ti and Ce were shifted toward lower particle size, as they are affected by industrial emissions at the Ferrara site. The Al and TB doses contribution to $D^{Tot}_{Tot}(an.)$ are consequently higher than for their insoluble fraction, especially at the Ferrara site (Figures S6–S8 of supplementary material).

3.4. Aerosol Respiratory Doses from Industrial Emissions

The soluble fractions of As, Ni, and Cr can be considered reliable tracers of anthropic combustion sources, including industrial emissions [20]. Figure 4 reports $D^R(an., d_{ai})$ and $D^{Tot}(an., d_{ai})$ size distributions together with the $D^R_{Tot}(an.)$ and $D^{Tot}_{Tot}(an.)$ doses, for the As soluble fractions after 1 h exposure at the Rome and Ferrara sites. The relevant doses for Ni and Cr are reported in Figures S9 and S10 of supplementary material. At both sites the main modes of $D^{Tot}(an., d_{ai})$ doses of such elements were in the fine ragion, with maxima at 0.56–1.0 μm and 1.0–1.8 μm, respectively at the Rome and Ferrara sites. Moreover, $D^{Tot}_{Tot}(an.)$ were higher at the Ferrara site due to industrial emissions: 0.20 ng, 0.14 ng and 0.37 ng at the Ferrara site and 0.09 ng, 0.06 ng and 0.32 ng, at the Rome site, respectively for As, Cr and Ni and As. A minor $D^{Tot}(an., d_{ai})$ mode in the coarse region was also present for the three elements at both sites, probably due to the soluble contribution of road re-suspended dust. Indeed, $D^{Tot}(an., d_{ai})$ of the insoluble fractions of the three elements (Figures S11–S13 of the supplementary material) have modes in the coarse region with maxima at 3.2–5.6 μm, with the exception of As at the Ferrara site (maximum at 1.8–3.2 μm). The main contribution to such doses is due to coarse road dust. Therefore, higher $D^{Tot}_{Tot}(an.)$ doses were estimated for the Rome site, due to the more intense dust re-suspension caused by the higher vehicular traffic than at the Ferrara site. After 1 h exposure 5.25 ng, 1.18 ng, 0.09 ng at the Rome site and 2.87 ng, 0.90 ng, 0.08 ng at the Ferrara site, respectively for the insoluble fractions of Cr, Ni and As, were deposited into the respiratory system. It is worth observing that differently from Cr and Ni, $D^{Tot}_{Tot}(As)$ was comparble at the two sites. This is due to relevance of a $D^{Tot}(As, d_{ai})$ fine mode centered at 0.56–1.0 μm at the Ferrara site that probably comes from the insoluble contribution of industrial emissions. As a consequence, $D^{TB}_{Tot}(As)$ and $D^{Al}_{Tot}(As)$ are more than two-fold higher at the Ferrara than at the Rome site. On the contrary, the higher contribution from resuspended dust at the Rome site lead to an increase of $D^H_{Tot}(As)$.

These results are of particular concern as inhalation exposure to As, Ni and Cr were proved to be correlated with human respiratory diseases. Indeed, a recent systematic review of inorganic As and respiratory health reported that inorganic As is the group 1 lung carcinogen active by both inhalation and ingestion; besides, the same review reported a strong evidence between arsenic exposure and non-malignant respiratory diseases, including respiratory symptoms and lung function impairment, acute respiratory tract infections, and an increase of non-malignant lung illness mortality [21]. Besides, a toxicological overview of Ni highlighted that the respiratory system is the primary target of Ni-related toxicity following inhalation of Ni and its compounds. In particular, respiratory disorders and diseases such as rhinitis, sinusitis, asthma, chronic bronchitis, emphysema and nasal septal perforations, hyposmia or anosmia and pulmonary changes with fibrosis were observed in workers exposed to Ni or nickel compounds [22]. Respiratory diseases associated with Ni exposure can be explained by the toxicity and the proinflammatory responses of airway epithelial cells experimentally evidenced for Ni, Cr, and other metals. As regards Cr, scientific evidence demonstrated that the human respiratory tract is a major target of inhalation exposure to Cr compounds [23].
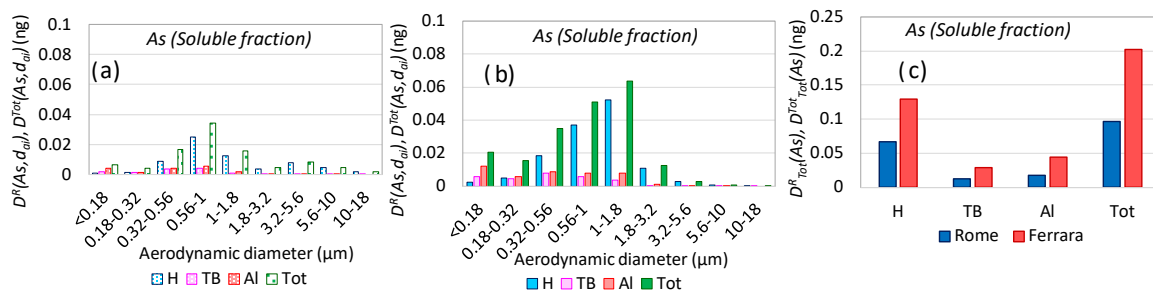
Figure 4. D^R (*As*, d_{ai}) and D^{Tot} (*As*, d_{ai}) doses at the Rome (**a**) and Ferrara (**b**) sites, relevant $D^R_{Tot}(As)$ and $D^{Tot}_{Tot}(As)$ doses (**c**) for As soluble fraction.

3.5. Aerosol Respiratory Doses from Secondary Inorganic Aerosol

NO_3^-, SO_4^{2-} and NH_4^+ are the main components of secondary aerosol and their impact on the aerosol respiratory doses is considerably different at the two site, because they are strongly influenced by their different meteo-climatic conditions. The poor degree of atmospheric remixing in the Po Valley during winter season, together with the important ammonia emissions from livestock farming, favor the formation of ammonium nitrate and the build up of its atmospheric concentrations. Consequently, considerably higher $D^{Tot}_{Tot}(NO_3^-)$ and $D^{Tot}_{Tot}(NH_4^+)$ doses were estimated for the Ferrara than for the Rome site (Figures 5c and 6c): 4345 ng, 1361 ng at the Ferrara site and 1878 ng, 231 ng at the Rome site, respectively for NO_3^- and NH_4^+. Two modes were present in the $D^{Tot}(NO_3^-, d_{ai})$ size distribution at the Ferrara site (Figure 5c): a main fine one with maximum at 1.0–1.8 μm and a minor coarse one centered at 3.2–5.6 μm. On the contrary, at the Rome site the fine mode was almost negligible and $D^{Tot}(NO_3^-, d_{ai})$ was almost completely present in the coarse mode (Figure 5a). Such mode is reasonably due to the interaction of nitric acid with sea salt aerosol that is frequently advected over Rome [24,25], with the consequent formation of volatile hydrochloric acid and coarse sodium nitrate.
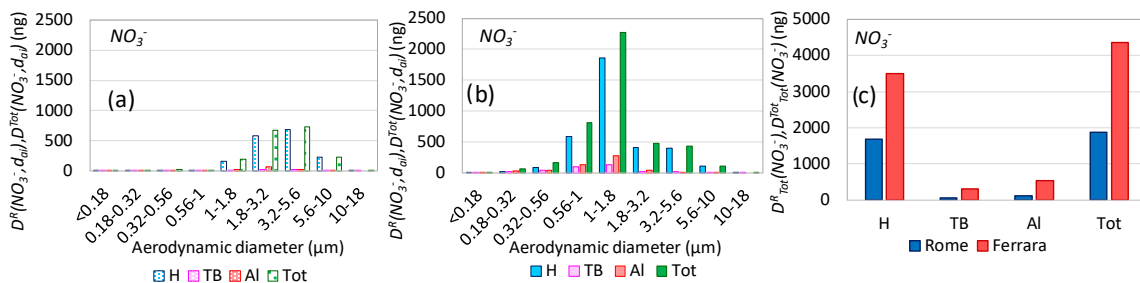
Figure 5. $D^R(NO_3^-, d_{ai})$ and $D^{Tot}(NO_3^-, d_{ai})$ doses at the Rome (**a**) and Ferrara (**b**) sites, relevant $D^R_{Tot}(NO_3^-)$ and $D^{Tot}_{Tot}(NO_3^-)$ doses (**c**).
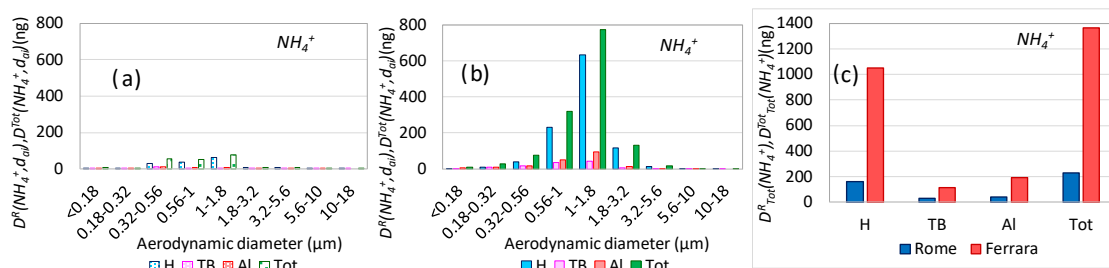
Figure 6. $D^R(NH_4^+, d_{ai})$ and $D^{Tot}(NH_4^+, d_{ai})$ doses at the Rome (**a**) and Ferrara (**b**) sites, relevant $D^R_{Tot}(NH_4^+)$ and $D^{Tot}_{Tot}(NH_4^+)$ doses (**c**).

As regards sulphate, $D_{Tot}^{Tot}(SO_4^{2-})$ was higher at the Rome than at the Ferrara site, respectively 949 ng and 772 ng (Figure 7c). The relevant $D^{Tot}(SO_4^{2-}, d_{ai})$ size distribution were both in the fine mode with a maximum at 1.0–1.8 μm and were very similar to the NH_4^+ size distributions, given that SO_4^{2-} was very likely present as ammonium sulphate at the two sites.
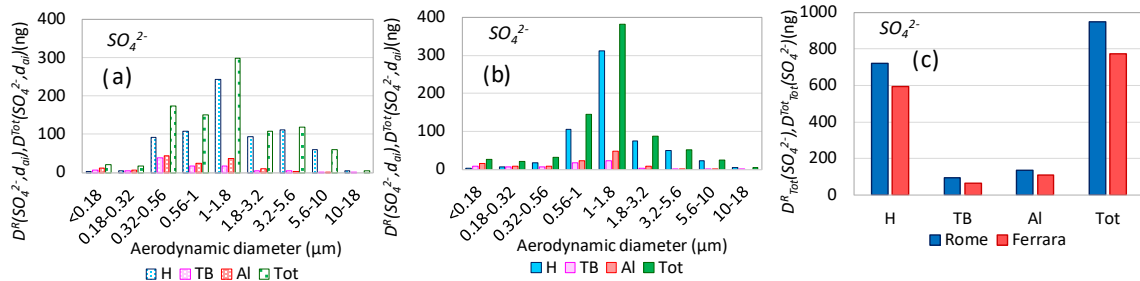

Figure 7. $D^R(SO_4^{2-}, d_{ai})$ and $D^{RTot}(SO_4^{2-}, d_{ai})$ doses at the Rome (**a**) and Ferrara (**b**) sites, relevant $D_{Tot}^R(SO_4^{2-})$ and $D_{Tot}^{Tot}(SO_4^{2-})$ doses (**c**).

3.6. Aerosol Respiratory Doses from Biomass Burning

The contribution of biomass burning to PM has increased over recent years and many studies have addressed its important adverse effects on human health [26]. Therefore, the assessment of respiratory doses of aerosol emitted from this source is a highly relevant task. Figure 8 shows $D^R(an., d_{ai})$ and $D^{Tot}(an., d_{ai})$ size distributions together with the $D_{Tot}^R(an.)$ and $D_{Tot}^{Tot}(an.)$ doses, for a reliable tracer of biomass burning, the soluble fraction of Rb, after 1 h exposure at the Rome and Ferrara sites. The same doses for K^+ are reported in Figure S14 (supplementary materials). $D_{Tot}^{Tot}(an.)$ doses were almost similar at the two sites: 115 ng, 0.33 ng at the Rome site and 119 ng, 0.31 ng at the Ferrara site, respectively for K and Rb (soluble fraction). The relevant $D^{Tot}(an., d_{ai})$ as well, were similar at the two sites with a main fine mode (maximum at 0.56–1.0 μm) due to biomass burning and a minor coarse mode (maximum at 3.2–5.6 μm) due to crustal material, for both elements. This occurrence suggests that the impact of biomass burning aerosol was similar at the two sites, showing a low influence of the ageing process.
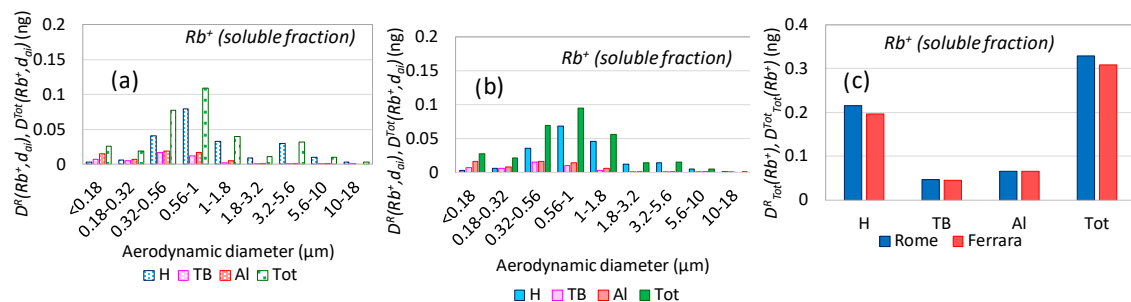

Figure 8. $D^R(Rb, d_{ai})$ doses at the Rome (**a**) and Ferrara (**b**) sites, relevant $D_{Tot}^R(Rb)$ and $D_{Tot}^{Tot}(Rb)$ doses (**c**) for rubidium soluble fraction.

3.7. Oxidative Potential Respiratory Doses

Figures 9–11 show $D^R(OP, d_{ai})$ and $D^{Tot}(OP, d_{ai})$ size distributions together with the $D_{Tot}^R(OP)$ and $D_{Tot}^{Tot}(OP)$ doses, for OP^{DCFH}, OP^{DTT} and OP^{AA} assays after 1 h exposure at the Rome and the Ferrara sites.

$D^R(AA, d_{ai})$ and $D^{Tot}(AA, d_{ai})$ displayed the same dimensional profile at the two site: a negligible response below about 1 μm and a coarse mode (maximum at 3.2–5.6 μm), suggesting sensitivity toward redox active components in coarse aerosol, namely to redox active components released by brake abrasion, such as Cu and Fe, to whom OP^{AA} assays is known to be sensitive [14,27–30].
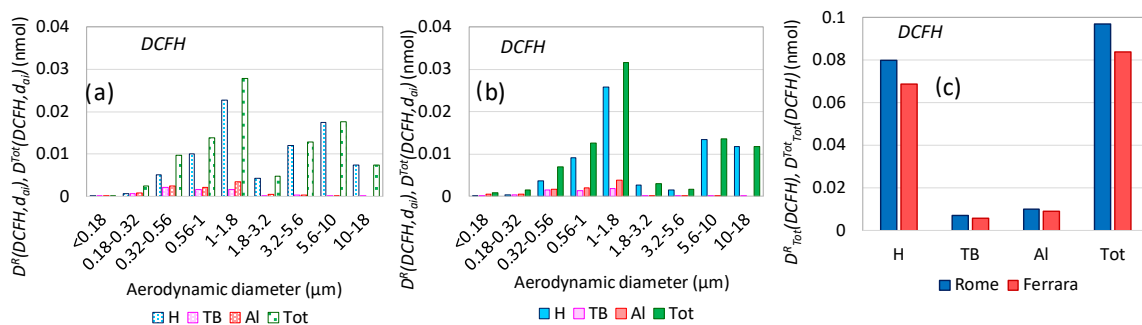
Figure 9. $D^R(DCFH, d_{ai})$ and $D^{Tot}(DCFH, d_{ai})$ doses at the Rome (**a**) and Ferrara (**b**) sites, relevant $D^R_{Tot}(DCFH)$ and ($D^{Tot}_{Tot}(DCFH)$ doses (**c**), for OP^{DFFH} assay.
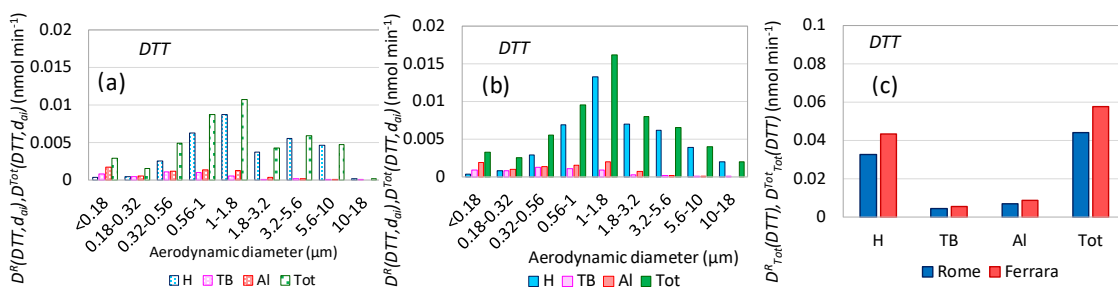

Figure 10. $D^R(DTT, d_{ai})$ and $D^{Tot}(DTT, d_{ai})$ doses at the Rome (**a**) and Ferrara (**b**) sites, relevant $D^R_{Tot}(DTT)$ and ($D^{Tot}_{Tot}(DTT)$ doses (**c**), for OP^{DTT} assay.
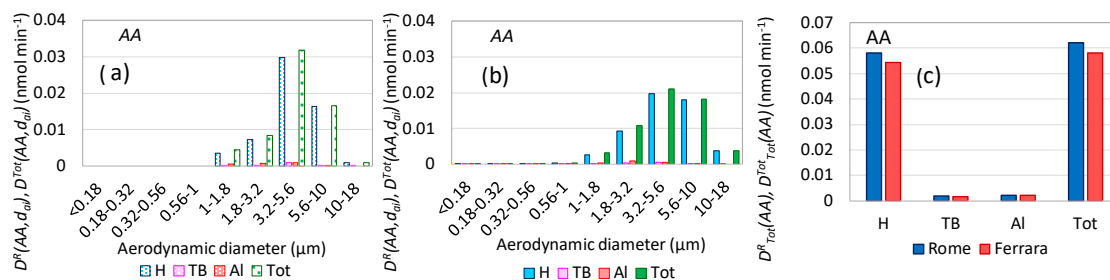

Figure 11. $D^R(AA, d_{ai})$ and $D^{Tot}(AA, d_{ai})$ doses at the Rome (**a**) and Ferrara (**b**) sites, relevant $D^R_{Tot}(AA)$ and ($D^{Tot}_{Tot}(AA)$ doses (**c**), for OP^{AA} assay.

At both sites $D^R(OP, d_{ai})$ and $D^{Tot}(OP, d_{ai})$ for DCFH and DTT assays shared almost the same size distributions in the fine mode, with a maximum at 1.0–1.8 μm. In particular, $D^{Tot}(OP, d_{ai})$ size distributions (Figure 10a,b) are in agreement with Fang et al. [31] who reported unimodal water-soluble OP^{DTT} peaked near 1–2.5 μm. OP^{DTT} and OP^{DCFH} elicited greater sensibility toward redox active component distributed in the fine mode, namely aerosol from biomass burning and anthropic combustion sources. Differences between the two OP doses were more evident in the coarse region, where $D^{Tot}(DCFH, d_{ai})$ and $D^{Tot}(DTT, d_{ai})$ showed a minor mode with maxima respectively at 5.6–10 μm and at 3.2–5.6 μm. OP^{DCHF} was more sensitive above 5 μm and less sensitive below, in comparison with OP^{DTT}. The differences between the two tests were evident in terms of total $D^R_{Tot}(OP)$ and $D^{Tot}_{Tot}(OP)$ doses as well. $D^R_{Tot}(DTT)$ and $D^{Tot}_{Tot}(DTT)$ were higher at the Ferrara than at the Rome site, whereas the contrary happened for OP^{DCHF}. Considering the similar $D^R_{Tot}(an.)$ and $D^{Tot}_{Tot}(an.)$ doses for tracers of biomass burning (K and Rb, soluble fraction) at the two sites, such difference seems to be mainly ascribed to the industrial emissions. Conversely, it is worth observing that although $D^{Tot}_{Tot}(NO_3^-)$ was considerably higher at the Ferrara (4345 ng) than at the Rome site (1878 ng), $D^{Tot}_{Tot}(DCFH)$ and $D^{Tot}_{Tot}(DTT)$ differences between the two site were of considerably lower entity. It is known that airborne PM contains variable amounts of water that can reach concentrations over 20 μg m^{-3} [32]. The redox potential of species such as NO$_3^-$ is strongly influenced by the acidity

of the liquid phase and increases, with decreasing pH. Given that the measured pH value of the soluble fraction of the collected PM was about 5, very likely the water phase adsorbed on PM was mildly acidic. Such occurrence probably determined the negligible redox activity of NO_3^- at the two sites.

Even if the DTT and the DCFH assays were more sensible toward fine PM, the contribution of particles below 0.18 μm was of low entity for both assays. Consequently, the highest percentage of $D_{Tot}^{Tot}(DCFH)$ and $D_{Tot}^{Tot}(DTT)$ (from 74% to 82%) was deposited in the head region rather than in the alveolar region, where UFPs more abundantly deposit [33]. On the other hand, it has been widely recognized that the ability of ultrafine particles (<0.1 μm) in generating higher level of ROS stems from their higher surface area per unit mass and from their surface reactivity [34]. This discrepancy could be overcome by referring $D^{Tot}(DCFH, d_{ai})$ and $D^{Tot}(DTT, d_{ai})$ to the unit mass doses $D^{Tot}(m, d_{ai})$. However, the low measured values of OPs and the low PM mass collected at the < 0.18 μm stage cause an increase of the measurement uncertainty that would expand when their ratio is calculated. The obtained results would be then scarcely reliable. Such occurrence should be considered to be one of the limits of the predictive capabilities of OP assays and need to be further investigated.

Furthermore, on interpreting these data it should be taken into account that their comprehension may be complex, due to the possible interplay of redox active components of PM. Indeed, Wang et al. [35] reported that the OP of copper significantly decreases upon mixing with 1,2-naphthoquinone, 2,3-dihydroxynaphthalene, and secondary organic aerosol (SOA) formed from the photooxidation naphthalene and phenanthrene. Transition metals [36,37] and humic-like substances [38] were widely considered and reported to contribute separately to the OP of PM; however, Lin et al. [39] showed that their interaction may be antagonistic or synergistic, depending on the metal and its concentration. Moreover, complexation reactions between organic ligand and metals may also occur [40]. Such reactions, depending on whether they increase or decrease the concentration ratio of the oxidized to the reduced form of the redox active species, cause an increase or a decrease of their redox potential. Due to the long sampling time (2–3 weeks), it should be considered that all these interactions may also have occurred on the membrane filter, upon accumulation of redox active species and metal chelating ligands and following the partitioning and oxidation of semi volatile organic compounds into the water phase adsorbed on PM.

4. Conclusions

Size-segregated measurements of metal, inorganic ions and oxidative potential had been carried out at an urban and at an industrial site. The OP of the PM soluble fractions had been assessed by AA, DTT and DCFH assays. Based on these data, the relevant doses deposited into the H, TB and Al regions of the respiratory system were estimated in this work. Different source tracers were adopted to address the contribution of the main emission sources present at the two sampling sites; namely dust brake emissions, soil dust resuspension, anthropic combustion, including industrial emissions and secondary inorganic aerosol. Metal doses were to greater extent distributed in the H region, because of the important deposition of both fine and coarse particles in such region. Total $D_{Tot}^{Tot}(an.)$ doses of tracers deriving from brake and soil re-suspension emissions were higher at the urban than at the industrial site. On the contrary, the relevant $D_{Tot}^{Tot}(an.)$ doses of fine PM components, which contain mainly soluble species, were comparable at the two sites or higher at the industrial site. Due to the higher capability of fine particles to penetrate beyond the H region, the doses deposited in the TB and Al regions increased for the tracers of combustive and secondary sources.

In particular, $D_{Tot}^{Tot}(an.)$ doses for the tracers of anthropic combustion (soluble fractions of As, Cr and Ni) were mainly distributed in the fine mode and were higher at the industrial site, due to the higher emissions from industrial settlements. The peculiar topography and meteo-climatic characteristics of the Po basin strongly favored the pollutant stagnation and the formation of secondary aerosol. Thus, $M_{Tot}^{Tot}(NO_3^-)$ and $M_{Tot}^{Tot}(NH_4^+)$ were by far higher at the industrial site in the Po valley, also due to ammonia emissions from livestock farming. $D_{Tot}^{Tot}(SO_4^{2-})$ was instead higher at the urban site. All the $D^{Tot}(an, d_{ai})$ doses for secondary aerosol mainly distributed in the fine mode with the exception of

$D^{Tot}\left(NO_3^-, d_{ai}\right)$ at the Rome site, where it was mainly distributed in the coarse mode, due to the reaction of nitric acid with sea salt aerosol. The impact of biomass burning was mainly observed in the fine mode and was similar at the two sites.

The mixture of the aerosols deriving from such different emission sources concurs to determine the oxidative potential of PM. The most striking characteristic of the three assays is their completely different responsiveness to the PM components. $D^R(AA, d_{ai})$ and $D^{Tot}(AA, d_{ai})$ are almost unaffected by fine mode aerosol, therefore by combustion emission and by biomass burning, whereas they respond to coarse aerosol (brake dust emissions and soil re-suspension).

On the contrary, $D^R(DTT, d_{ai})$, $D^{Tot}(DTT, d_{ai})$, $D^R(DCFH, d_{ai})$ and $D^{Tot}(DCFH, d_{ai})$ are mainly determined by the OP related to fine mode particles and to minor extent, with some differences between the two assays, by OP of coarse PM. Indeed, their size distribution matched the size distribution of biomass burning and of combustion aerosols. Therefore, AA could be considered appropriate to address the ROS generation of aerosol that mainly deposit in the H region, whereas DTT and DCFH would be more suitable to emphasize oxidative activity in the TB and Al region. However, there are some discrepancies in the OP dose in the ultrafine region, in particular for DCFH assay. The relevant $M^{Tot}(DCFH, d_{ai})$, particularly at the urban site, seems to have no sensitivity to this size of particles. It is not clear whether such occurrence is due to an intrinsic lack of response toward the redox active components in this size fraction or it may possibly arise from non-additive interactions of redox active components and/or from their modification on the filter surface. This point deserves further investigations, considering that UFPs, due to their surface reactivity, are known to importantly contribute to ROS generation capability of atmospheric PM.

References

1. Hamanaka, R.B.; Mutlu, G.M. Particulate matter air pollution: Effects on the cardiovascular system. *Front. Endocrinol.* **2018**, *9*, 680. [CrossRef]

2. Abdolahnejad, A.; Jafari, N.; Mohammadi, A.; Miri, M.; Hajizadeh, Y.; Nikoonahad, A. Cardiovascular, respiratory, and total mortality ascribed to PM_{10} and $PM_{2.5}$ exposure in Isfahan, Iran. *J. Educ. Health Promot.* **2017**, *6*, 109. [CrossRef]

3. Anderson, J.O.; Thundiyil, J.G.; Stolbach, A. Clearing the air: A review of the effects of particulate matter air pollution on human health. *J. Med. Toxicol.* **2012**, *8*, 166–175. [CrossRef] [PubMed]

4. Li, Z.; Tang, Y.; Song, X.; Lazar, L.; Li, Z.; Zhao, J. Impact of ambient PM2.5 on adverse birth outcome and potential molecular mechanism. *Ecotoxicol. Environ. Saf.* **2019**, *169*, 248–254. [CrossRef] [PubMed]

5. IARC. Working Group on the Evaluation of Carcinogenic Risks to Humans. Outdoor Air Pollution. *IARC Monogr. Eval. Carcinog. Risks Hum.* **2016**, *109*, 9.

6. Fang, T.; Lakey, P.S.J.; Weber, R.J.; Shiraiwa, M. Oxidative potential of particulate matter and generation of reactive oxygen species in epithelial lining fluid. *Environ. Sci. Technol.* **2019**. [CrossRef] [PubMed]

7. Bates, J.T.; Fang, T.; Verma, V.; Zeng, L.; Weber, R.J.; Tolbert, P.E.; Abrams, J.Y.; Sarnat, S.E.; Klein, M.; Mulholland, J.A.; et al. Review of acellular assays of ambient particulate matter oxidative potential: Methods and relationships with composition, sources, and health effects. *Environ. Sci. Technol.* **2019**, *53*, 4003–4019. [CrossRef]

8. Manigrasso, M.; Protano, C.; Vitali, M.; Avino, P. Where do ultrafine particles and nano-sized particles come from? *J. Alzheimers Dis.* **2019**, *68*, 1371–1390. [CrossRef]

9. EPA, U. *Air Quality Criteria for Particulate Matter (Final Report, Oct 2004)*; Environmental Protection Agency: Washington, DC, USA, 2004.

10. Manigrasso, M.; Vitali, M.; Protano, C.; Avino, P. Ultrafine particles in domestic environments: Regional doses deposited in the human respiratory system. *Environ. Int.* **2018**, *118*, 134–145. [CrossRef]

11. Simonetti, G.; Conte, E.; Perrino, C.; Canepari, S. Oxidative potential of size-segregated PM in an urban and an industrial area of Italy. *Atmos. Environ.* **2018**, *187*, 292–300. [CrossRef]

12. Canepari, S.; Perrino, C.; Astolfi, M.L.; Catrambone, M.; Perret, D. Determination of soluble ions and elements in ambient air suspended particulate matter: Inter-technique comparison of XRF, IC and ICP for sample-by-sample quality control. *Talanta* **2009**, *77*, 1821–1829. [CrossRef] [PubMed]

13. Astolfi, M.L.; Marconi, E.; Protano, C.; Vitali, M.; Schiavi, E.; Mastromarino, P.; Canepari, S. Optimization and validation of a fast digestion method for the determination of major and trace elements in breast milk by ICP-MS. *Anal. Chim. Acta* **2018**, *1040*, 49–62. [CrossRef] [PubMed]

14. Crobeddu, B.; Aragao-Santiago, L.; Bui, L.C.; Boland, S.; Squiban, A.B. Oxidative potential of particulate matter 2.5 as predictive indicator of cellular stress. *Environ. Pollut.* **2017**, *230*, 125–133. [CrossRef] [PubMed]

15. Manigrasso, M.; Protano, C.; Vitali, M.; Avino, P. Nanoparticle behaviour in an urban street canyon at different heights and implications on indoor respiratory doses. *Atmosphere* **2019**, *10*, 772. [CrossRef]

16. Asgharian, B.; Hofmann, W.; Bergmann, R. Particle deposition in a multiple path model of the human lung. *Aerosol Sci. Technol.* **2009**, *34*, 332–339. [CrossRef]

17. ICRP. *Publication 66: Human Respiratory Tract Model for Radiological Protection, International Commission on Radiological Protection (ICRP)*; Elsevier Science: Oxford, UK, 1994.

18. Canepari, S.; Astolfi, M.L.; Catrambone, M.; Frasca, D.; Marcoccia, M.; Marcovecchio, F.; Massimi, L.; Rantica, E.; Perrino, C. A combined chemical/size fractionation approach to study winter/summer variations, ageing and source strength of atmospheric particles. *Environ. Pollut.* **2019**, *253*, 19–28. [CrossRef]

19. Vecchi, R.; Marcazzan, G.; Valli, G.; Ceriani, M.; Antoniazzi, C. The role of atmospheric dispersion in the seasonal variation of PM1 and PM2.5 concentration and composition in the urban area of Milan (Italy). *Atmos. Environ.* **2004**, *38*, 4437–4446. [CrossRef]

20. Canepari, S.; Astolfi, M.L.; Farao, C.; Maretto, M.; Frasca, D.; Marcoccia, M.; Perrino, C. Seasonal variations in the chemical composition of particulate matter: A case study in the Po Valley. Part II: Concentration and solubility of micro-and trace-elements. *Environ. Sci. Pollut. Res.* **2014**, *21*, 4010–4022. [CrossRef]

21. Sanchez, T.R.; Perzanowski, M.; Graziano, J.H. Inorganic arsenic and respiratory health, from early life exposure to sex-specific effects: A systematic review. *Environ Res.* **2016**, *147*, 537–555. [CrossRef]

22. Public Health England. *Nickel, Toxicological Overview, Toxicology Department CRCE, PHE 2009, Version 1*; Public Health England: London, UK, 2009.

23. Wilbur, S.; Abadin, H.; Fay, M.; Yu, D.; Tencza, B.; Ingerman, L.; Klotzbach, J.; James, S. *Toxicological Profile for Chromium*; Atlanta (GA) Agency for Toxic Substances and Disease Registry (US): Atlanta, GA, USA, 2012.

24. Manigrasso, M.; Abballe, F.; Jack, R.F.; Avino, P. Time-resolved measurement of the ionic fraction of atmospheric fine particulate matter. *J. Chromatogr. Sci.* **2010**, *48*, 549–552. [CrossRef]

25. Perrino, C.; Canepari, S.; Catrambone, M.; Dalla Torre, S.; Rantica, E.; Sargolini, T. Influence of natural events on the concentration and composition of atmospheric particulate matter. *Atmos. Environ.* **2009**, *43*, 4766–4779. [CrossRef]

26. Corsini, E.; Marinovich, M.; Vecchi, R. Ultrafine particles from residential biomass combustion: A review of experimental data and toxicological response. *Int. J. Mol. Sci.* **2019**, *20*, 4992. [CrossRef] [PubMed]

27. Simonetti, G.; Conte, E.; Massimi, L.; Frasca, D.; Perrino, C.; Canepari, S. Oxidative potential of particulate matter components generated by specific emission sources. *J. Aerosol Sci.* **2018**, *126*, 99–109. [CrossRef]

28. Gonzalez, D.H.; Cala, C.K.; Peng, Q.; Paulson, S.E. HULIS enhancement of hydroxyl radical formation from Fe (II): Kinetics of fulvic acid–Fe (II) complexes in the presence of lung antioxidants. *Environ. Sci. Technol.* **2017**, *51*, 7676–7685. [CrossRef]

29. Campbell, S.J.; Utinger, B.; Lienhard, D.M.; Paulson, S.E.; Shen, J.; Griffiths, P.T.; Stell, A.C.; Kalberer, M. Development of a Physiologically Relevant Online Chemical Assay To Quantify Aerosol Oxidative Potential. *Anal. Chem.* **2019**, *91*, 13088–13095. [CrossRef]

30. Godri, K.J.; Harrison, R.M.; Evans, T.; Baker, T.; Dunster, C.; Mudway, I.S.; Kelly, F.J. Increased oxidative burden associated with traffic component of ambient particulate matter at roadside and urban background schools sites in London. *PLoS ONE* **2011**, *6*, e21961. [CrossRef]

31. Fang, T.; Zeng, L.; Gao, D.; Verma, V.; Stefaniak, A.B.; Weber, R.J. Ambient size distributions and lung deposition of aerosol dithiothreitol-measured oxidative potential: Contrast between soluble and insoluble particles. *Environ. Sci. Technol.* **2017**, *51*, 6802–6811. [CrossRef]

32. Canepari, S.; Farao, C.; Marconi, E.; Giovannelli, C.; Perrino, C. Qualitative and quantitative determination of water in airborne particulate matter. *Atmos. Chem. Phys.* **2013**, *13*, 1193–1202. [CrossRef]

33. Manigrasso, M.; Vernale, C.; Avino, P. Traffic aerosol lobar doses deposited in the human respiratory system. *Environ. Sci. Pollut. Res. Int.* **2017**, *24*, 13866–13873. [CrossRef]

34. Oberdörster, G.; Oberdörster, E.; Oberdörster, J. Nanotoxicology: An emerging discipline evolving from studies of ultrafine particles. *Environ. Health Perspect.* **2005**, *113*, 823–839. [CrossRef]

35. Wang, S.; Ye, J.; Soong, R.; Wu, B.; Yu, L.; Simpson, A.J.; Chan, A.W. Relationship between chemical composition and oxidative potential of secondary organic aerosol from polycyclic aromatic hydrocarbons. *Atmos. Chem. Phys.* **2018**, *18*, 3987–4003. [CrossRef]

36. Shafer, M.M.; Perkins, D.A.; Antkiewicz, D.S.; Stone, E.A.; Quraishi, T.A.; Schauer, J.J. Reactive oxygen species activity and chemical speciation of size-fractionated atmospheric particulate matter from Lahore, Pakistan: An important role for transition metals. *J. Environ. Monit.* **2010**, *12*, 704–715. [CrossRef] [PubMed]

37. Rodrigo-Moreno, A.; Poschenrieder, C.; Shabala, S. Transition metals: A double edge sward in ROS generation and signaling. *Plant Signal Behav.* **2013**, *8*, e23425. [CrossRef] [PubMed]

38. Lin, P.; Yu, J.Z. Generation of reactive oxygen species mediated by humic-like substances in atmospheric aerosols. *Environ. Sci. Technol.* **2011**, *45*, 10362–10368. [CrossRef] [PubMed]

39. Lin, M.; Yu, J.Z. Effect of metal-organic interactions on the oxidative potential of mixtures of atmospheric humic-like substances and copper/manganese as investigated by the dithiothreitol assay. *Sci. Total Environ.* **2019**, *697*, 134012. [CrossRef]

40. Paris, R.; Desboeufs, K.V. Effect of atmospheric organic complexation on iron-bearing dust solubility. *Atmos. Chem. Phys.* **2013**, *13*, 4895–4905. [CrossRef]